

Spotlight Selection | Food Microbiology | Full-Length Text

Salmonella dry surface biofilm: morphology, single-cell landscape, and sanitization

Zeja Lin,¹ Zhiqian Liang,¹ Shuang He,¹ Fion Wei Lin Chin,¹ Dejian Huang,^{1,2} Yi Hong,³ Xiang Wang,³ Dan Li^{1,2}**AUTHOR AFFILIATIONS** See affiliation list on p. 17.

ABSTRACT In this study, *Salmonella* Typhimurium dry surface biofilm (DSB) formation was investigated in comparison with wet surface biofilm (WSB) development. Confocal laser scanning microscopic analysis revealed a prominent green cell signal during WSB formation, whereas a red signal predominated during DSB formation. Electron microscopy was also used to compare the features of DSB and WSB. Overall, WSB was unevenly scattered over the surface, whereas DSB was evenly dispersed. In contrast to WSB cells, which have a distinct plasma membrane and outer membrane layer, DSB cells are contained in large capsules and compressed. Next, microbiome single-cell transcriptomics was used to investigate the functional heterogeneity of the *Salmonella* DSB microbiome, with nine clusters successfully identified. Although over 60% of the dried cells were metabolically inactive, the rest of the *Salmonella* cells still demonstrated specific antioxidative and virulence capabilities, suggesting a possible concern for low-moisture food (LMF) safety. Finally, because sanitization in LMF industries must be conducted without water, a list of 39 flavonoids was tested for their combined effect with 70% isopropyl alcohol (IPA) against DSB, and morin induced the greatest reduction in the green:red ratio from 3.67 to 0.43. Significantly higher reductions of *Salmonella* viability in DSB were achieved by 10-, 100-, 1,000-, and 10,000- $\mu\text{g}/\text{mL}$ morin (1.69 ± 0.25 , 3.21 ± 0.23 , 4.32 ± 0.24 , and 5.18 ± 0.16 log CFU/sample reductions) than 70% IPA alone (1.55 ± 0.20 log CFU/sample reduction) ($P < 0.05$), indicating the potential to be formulated as a dry sanitizer for the LMF industry.

IMPORTANCE DSB growth of foodborne pathogens in LMF processing environments is associated with food safety, financial loss, and compromised consumer trust. This work is the first comprehensive examination of the characteristics of *Salmonella* DSB while exploring its underlying survival mechanisms. Furthermore, morin dissolved in 70% IPA was proposed as an efficient dry sanitizer against DSB to provide insights into biofilm control during LMF processing.

KEYWORDS *Salmonella*, dry surface biofilm, flavonoid, morin, dry sanitization

Recent recalls and outbreaks associated with low-moisture food (LMF) products have provided mounting evidence that bacterial pathogens can survive under desiccated conditions (1, 2). For example, *Salmonella* was found to be present in a grain factory for a minimum of 10 years, despite the lack of moisture and decreased metabolic activity (3). The incidence of *Salmonella* outbreaks associated with LMFs has steadily increased annually. In 2022, The Food and Drug Administration announced four recalls in the USA in March, May, August, and November 2021. These recalls were related to a variety of LMFs, such as flour, hummus, tahini, and potato chips. When present in food, *Salmonella* can form biofilms that enhance its ability to survive and resist various disinfection methods during food processing, increasing the risk of *Salmonella* causing foodborne illnesses (4–6). Although the ability of *Salmonella* to form biofilms

Editor Christopher A. Elkins, Centers for Disease Control and Prevention, Atlanta, Georgia, USAAddress correspondence to Dan Li,
dan.li@nus.edu.sg.

The authors declare no conflict of interest.

See the funding table on p. 17.

Received 16 August 2024**Accepted** 3 October 2024**Published** 4 November 2024Copyright © 2024 American Society for
Microbiology. All Rights Reserved.

in food processing environments has been well documented (7, 8), Alonso et al. (9) suggested that *Salmonella* may develop a distinct kind of dry surface biofilm (DSB) when it encounters a dry environment. Compared with traditional wet surface biofilm (WSB), DSBs are more difficult to detect and eliminate (10). When surfaces are moist, the organic molecules found in food processing or left over after sanitization cycles are carried and taken up by the surfaces. The creation of a conditioning film occurs, resulting in the subsequent production of a WSB (9). Similarly, while dry surfaces may seem dry with the naked eye, it is often possible to detect the presence of thin liquid films and tiny droplets, referred to as microscopic surface wetness. These microdroplets may provide a suitable environment for the development of DSB (11). Although there has been considerable research on the formation of foodborne pathogens in traditional WSB and their participation in food contamination, studies of these pathogens in dry environments, such as the growth pattern and morphology of DSB, as well as the tolerance of DSB to different sanitizers, are lacking. Consequently, these deficiencies underscore the necessity of conducting more extensive and inclusive research to better understand pathogenic biofilms in dry environments and to mitigate the hazards they present.

DSBs are most often found in dry food processing environments (9). Thus, minimizing the incorporation of water into sanitization procedures is critical for preventing moisture exposure and microbial contamination, emphasizing the need for an efficient waterless sanitizer against DSB. The most common dry sanitizers used in the food industry are alcohol-based sanitizers such as ethanol, isopropyl alcohol (IPA), and butanol (12). Alcohol-based sanitizers are efficient against vegetative cells but not spores or biofilms (13). Over the past few years, interest in the antimicrobial properties of flavonoids in relation to a variety of bacterial species has increased. For example, quercetin has been shown to exhibit bacteriostatic activity against various Gram-negative bacteria, including *Salmonella* and *Escherichia coli* (14). Myricetin and luteolin exhibit an inhibitory effect on *Pseudomonas aeruginosa* (15). Other flavonoids, including kaempferol, lucenin, apigenin, neohesperidin, and morin, were also identified as efficacious against a diverse array of Gram-negative and Gram-positive microorganisms (16). Owing to the high solubility of flavonoids in alcohol, these compounds exhibit significant potential for collaboration with alcohol-based sanitizers in the LMF industry.

This study aimed to investigate the characteristics of *Salmonella* DSB, including their biofilm growth pattern, sanitizer tolerance, and morphology, in comparison with those of WSB. In addition, recent advancements in single-cell microbiological RNA sequencing have allowed us to analyze the single-cell functional heterogeneity of DSB. This is crucial for understanding the presence of persister and heteroresistant subpopulations. Finally, a panel of flavonoids was evaluated for their effectiveness against DSB as potential dry sanitizers suitable for the LMF industry. With the efforts of this research, the food industry would benefit from the insight of dry biofilm management.

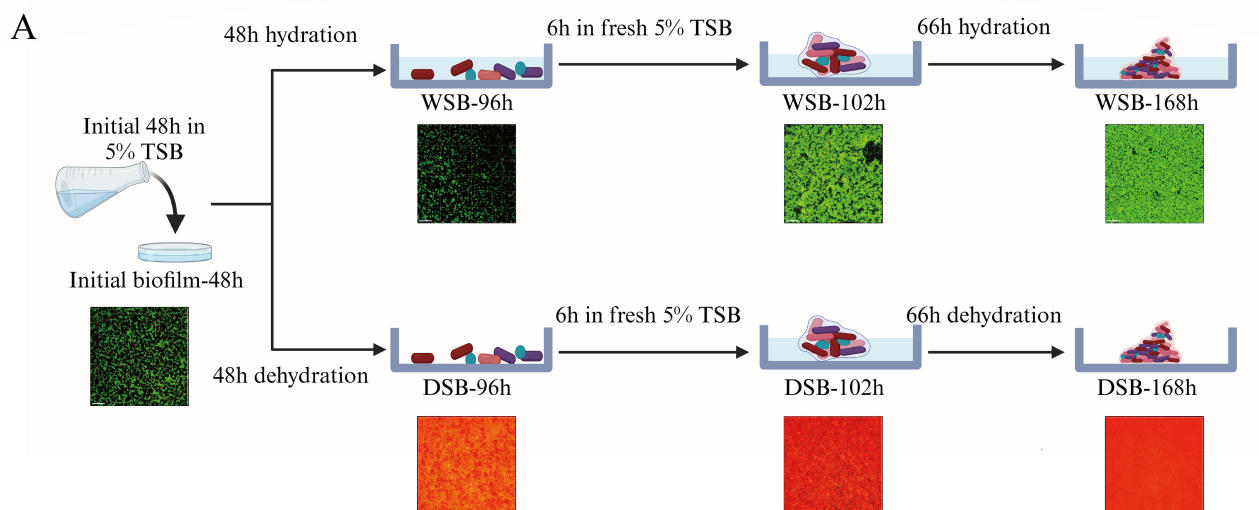
MATERIALS AND METHODS

Bacterial strains and culture conditions

The strain *Salmonella enterica* serovar Typhimurium ATCC 14028 was acquired from the ATCC. Before being used in the experiments, the stock culture was revived in tryptone soy broth (TSB; Sigma–Aldrich, USA) by incubation at 37°C overnight for two consecutive cycles. The stock was inoculated into 10 mL of fresh TSB (1:100, vol/vol) and incubated at 37°C overnight for every test. The cell pellets were generated by centrifuging the culture suspension at $4,500 \times g$ for 10 min after being rinsed twice with 0.1% peptone water (0.1% PW).

Development of WSB and DSB

The WSB and DSB formation protocol was adopted by Amaeze et al. (17) with some modifications. Figure 1A shows a schematic diagram of the development process for



B

	Green cells signal ($\times 10^3 \mu\text{m}^3$ biovolume)	Red cells signal ($\times 10^3 \mu\text{m}^3$ biovolume)	Total cells signal ($\times 10^3 \mu\text{m}^3$ biovolume)	Green cells (%)	Red cells (%)
Initial biofilm-48h	^C 389.95±23.79 _b	^F 57.40±3.65 _c	^D 447.36±27.44 _a	^B 87.17	^D 12.83
WSB-96h	^D 256.50±22.47 _b	^G 21.39±5.11 _c	^F 277.89±27.58 _a	^A 92.30	^E 7.70
WSB-102h	^A 703.36±43.28 _b	^D 105.94±6.27 _c	^A 809.29±49.55 _a	^B 86.91	^D 13.09
WSB-168h	^B 443.81±23.55 _b	^E 83.94±7.77 _b	^C 527.75±31.33 _a	^B 84.09	^D 15.91
Initial biofilm-48h	^C 389.95±23.79 _b	^F 57.40±3.65 _c	^D 447.36±27.44 _a	^B 87.17	^D 12.83
DSB-96h	^F 51.23±7.95 _c	^C 346.90±23.14 _b	^E 398.13±31.10 _a	^E 12.87	^A 87.13
DSB-102h	^D 218.12±14.88 _c	^A 566.66±13.00 _b	^A 784.78±27.87 _a	^C 27.79	^C 72.21
DSB-168h	^E 138.61±19.09 _c	^B 526.21±14.58 _b	^B 664.82±33.68 _a	^D 20.85	^B 79.15

Note: Data are presented as means ± standard deviation (n = 3). Values within each column preceded by different uppercase letters are significantly different ($P < 0.05$). Values within each row followed by different lowercase letters are significantly different ($P < 0.05$).

FIG 1 Flowchart of the protocol of *S. Typhimurium* WSB and DSB development (A), and profiles of green and red cell signals during the development of WSB and DSB (B).

both varieties of biofilm, which occurs at ambient temperature. In brief, the cell pellets obtained previously were resuspended in 5% TSB, and 1 mL was added to a Petri dish (60 × 15 mm) for 48 h. For WSB growth, the dish was hydrated for another 48 h, after which the liquid was discarded, and 1 mL of fresh 5% TSB was added for 6 h. Finally, the dish was hydrated for 66 h, and a 168-h-old WSB was prepared for the next experiment. For DSB growth, the sequential cycles of hydration phases and dehydration are depicted in Fig. 1A. Following the first 48 h in 5% TSB, the liquid was removed, and the dish was covered with a lid and kept in a desiccator with saturated K_2CO_3 solution, which maintained the relative humidity at 49% at ambient temperature, according to our preliminary data. The dish was dehydrated for 48 h and subsequently supplied with 1 mL of fresh 5% TSB for 6 h. The liquid was discarded once more, and the dish was kept dehydrated for the final 66 h to obtain 168-h-old DSB.

Monitoring of WSB and DSB growth

Confocal laser scanning microscopic (CLSM) analysis was carried out via a previously established method to visualize the changes in WSB and DSB during the growth process (18). Biofilm samples for CLSM imaging were generated as outlined in Development of WSB and DSB by cultivating 1 mL of bacterial culture on a confocal dish with a diameter

of 35 mm. The samples were stained via the Live/Dead BacLight Viability Kit L-7012 (Molecular Probes, Eugene, USA) according to the manufacturer's instructions. After staining, the WSB and DSB samples were evaluated immediately via an Olympus FV1000 laser scanning confocal microscope. The biofilms were imaged via a $\times 60$ water-immersion lens. The photos were processed via the "3D review" and "section" tools from IMARIS (v.9.0) software (Bitplane, Switzerland). BiofilmQ (<https://drescherlab.org/data/biofilmQ>) was used to measure the biovolume signals in WSB and DSB.

Evaluation of sanitizer tolerance between WSB and DSB

To compare the production of extracellular polymeric substances (EPSs), a crystal violet (CV) staining procedure was used with slight modifications (19). The WSB and DSB samples from "Development of WSB and DSB," above, were washed twice with deionized (DI) water to remove unattached cells. Each Petri dish was treated with 1 mL of DI water (control), 70% IPA, or 200- $\mu\text{g}/\text{mL}$ sodium hypochlorite for 1 min before adding 1 mL of buffered peptone to neutralize the sanitizer effect. The dish was dried, and 1 mL of CV (0.1%, wt/vol) was added for 30 min of staining. The excess CV mixture was then washed with DI water. The fixed CV was extracted by adding 1 mL of 96% ethanol and incubating for 15 min. The extracted sample was then transferred to a fresh 96-well plate to measure the absorbance at 590 nm. In addition, enumeration was conducted on WSB and DSB to verify the biomass results. Following the previously described sanitization and neutralization methods, the Petri dish was dried, and 1 mL of DI water was added. The attached samples were obtained by scraping with a cell scraper for 1 min. The suspension was then serially diluted and counted on tryptone soy agar (Sigma–Aldrich).

Electron microscopy imaging of WSB and DSB

Scanning electron microscopy (SEM) imaging was performed according to the methods of Santana et al. (20) with some modifications. Briefly, biofilm samples obtained from "Development of WSB and DSB," above, were immersed in 2.5% glutaraldehyde (Sigma–Aldrich) for fixation overnight. After fixation, the samples were rinsed thoroughly with phosphate-buffered saline (PBS) to remove any residual glutaraldehyde and then immersed in 1% osmium tetroxide (Sigma–Aldrich) for 1 h to further stabilize the sample structure and enhance contrast for electron microscopy. The samples were subsequently dehydrated through a graded ethanol series of 25%, 50%, 75%, 95%, and 100%; subjected to critical point drying (CPD300, Leica Microsystems); sputter coated with gold (ACE200, Leica Microsystems). Finally, SEM images were collected at 10 kV via a Quanta 650 FEG SEM (Thermo Fisher Scientific, USA).

The transmission electron microscopy (TEM) imaging procedure was performed according to the methods of Stirling (21) with some modifications. The biofilm samples from "Development of WSB and DSB," above, were also fixed in 2.5% glutaraldehyde, washed with PBS prior to being postfixed with 1% osmium tetroxide, and then dehydrated through an ethanol series as described in the SEM procedure. After that, the samples were infiltrated with Araldite resin (Sigma–Aldrich), embedded, and polymerized at 60°C for 24 h. The embedded samples were sectioned with an ultramicrotome (UC6, Leica Microsystems) into 100-nm slices, stained with lead citrate (Sigma–Aldrich), and imaged via a JEM1400Flash transmission electron microscope (JEOL Asia Pte Ltd.) at 100 kV.

Single-cell RNA sequencing of the DSB microbiome

A previously established method by Jia et al. (22), which included the use of a customized microfluidic barcoding platform, was adopted in this study. In brief, 168-h-old DSBs from "Development of WSB and DSB," above, were permeabilized and washed with 0.04% Tween-20 in PBS after being fixed in 4% PFA at 4°C overnight. Lysozyme was used to break down the cell wall, and the mixture was incubated for 15 min at 37°C. The bacteria were promptly rinsed and resuspended in PBS containing an RNase inhibitor (Thermo Fisher Scientific) after the cell wall digestion stage. Nucleic acid capture, single-cell partitioning and encapsulation, and microfluidic droplet formation

were accomplished via the VITAcruizer bacterium preparation apparatus DP400 (Cat # E20000131, M20 Genomics). Single-cell library construction, purification, and prelibrary sample processing were carried out via the VITApilote high-throughput formalin-fixed and paraffin-embedded (FFPE) single-cell transcriptome kit (Cat # R20123124, M20 Genomics). The equipment manuals and perspective kits were followed when the experiments were performed.

Single-stranded DNA was inhibited by permeabilizing and obstructing the bacterial suspension that had been prepared. The reverse transcription of total RNA within the cell was subsequently initiated by the addition of random primers. The cDNA fragments that were produced were subsequently ligated to adapters present within the bacteria. The barcode beads, which contained cell barcodes and barcode-unique molecular identifiers (UMIs), were combined with the reverse-transcribed single-bacteria suspension and reagents. A VITAcruizer DP400 instrument was employed to encapsulate, capture, and barcode the mixture. Barcoded cDNA strands were produced as a consequence of the extension of the resulting product. The resulting cDNA was employed as the template for PCR amplification. The purified products were subsequently employed to create a standard next-generation sequencing library following cDNA amplification. The single-cell library that was created was sequenced on an Xplus sequencer (Illumina) using 150-bp paired-end reads and contained P5 and P7 adapters. The sequencing and bioinformatic analysis were conducted on the platform of Majorbio Co., Ltd. (Shanghai, China).

The VITaseer (v.1.0) pipeline was employed to analyze the reads, with the default and recommended parameters. The primers and capture adapter sequences were initially removed from the unprocessed sequencing data. Then, for each Read 1, both the UMI (8 nts) and the cell-specific barcode (20 nts) were extracted and merged to create sequenced barcodes that can be uniquely ascribed to the same accepted barcode with a Hamming distance of 1 nts or less. The STAR module in STAR (v.2.7.10 a) was employed to construct the gene expression matrix via Read 2 (23). STARSO was employed to identify legitimate microorganisms. This output was subsequently incorporated into the Seurat (v.4.1.1) R toolkit for downstream analysis and quality control of the single-cell RNA sequencing data (24). Unless otherwise specified, all functions were executed with the default parameters. The matrices were initially filtered to eliminate low-quality cells via a standard panel of two quality criteria: (i) number of detected transcripts (number of unique molecular identifiers) and (ii) number of detected genes (numbers that exceeded the mean value by ± 2 standard deviations). The `percentageFeatureSet` function of the Seurat package was employed to determine the expression of mitochondrial genes (24). A subset of variable genes was extracted via normalization of the data via the `normalizeData` function in the Seurat package. While accounting for the robust correlation between variability and average expression, variable genes were identified. Following the identification of “anchors” between data sets via `FindIntegrationAnchors` and `IntegrateData` in the Seurat package (25), data were subsequently integrated from various samples. After that, the data were scaled, and principal component analysis (PCA) was conducted to reduce them to the top 30 PCA components. The clusters were represented on a two-dimensional map that was generated via uniform manifold approximation and projection (UMAP) (26).

The Louvain method (27) was employed to aggregate cells after a shared nearest neighbor graph was computed, utilizing graph-based clustering of the PCA-reduced data. The same procedure of scaling, dimensionality reduction, and clustering was applied to the specific set of data (typically restricted to one category of cell) for subclustering. The Wilcoxon rank-sum test was employed to identify significantly differentially expressed genes in each cluster in comparison to the remaining clusters. The cell type was determined via SCINA (28) and known marker genes.

The `FindMarkers` function in Seurat was employed to identify differentially expressed genes (DEGs) between two distinct samples or clusters via a likelihood ratio test. In essence, DEGs were regarded as significantly differentially expressed genes if their

$|\log_2FC|$ value was greater than 0.25 and their P_{adjust} value was less than 0.05. Furthermore, gene ontology (GO) and Kyoto Encyclopedia of Genes and Genomes (KEGG) functional enrichment analyses were conducted to determine which DEGs were substantially enriched in GO terms and metabolic pathways at a Bonferroni-corrected P value of ≤ 0.05 in comparison with the whole-transcriptome background. Goatools (<https://github.com/tanghaibao/Goatools>) was used to conduct GO functional enrichment analysis. Python SciPy software was used to conduct the KEGG functional enrichment analysis.

Evaluation of the antimicrobial effects of flavonoids against DSB

A list of flavonoids (see Fig. 6A), which were purchased from various sources, including Sigma–Aldrich, Indofine Chemical Company (USA), and Nanjing Yuanzhi Biotechnology Co. Ltd. (China), were tested against *Salmonella* DSB. A high-throughput screening method using the LIVE/DEAD viability kit (L-7012) was developed to evaluate their antimicrobial effectiveness (29). During the assay, the viability of *Salmonella* DSB in response to various flavonoids is presented as a ratio of green (viable) and red (dead) cells as follows (30):

$$\frac{\text{Green}}{\text{Red}} \text{ ratio} = \frac{\text{Fluorescence signal, emission 530 nm}}{\text{Fluorescence signal, emission 630 nm}}$$

In brief, all flavonoids were dissolved in 70% IPA to obtain a final concentration of 100 $\mu\text{g}/\text{mL}$. DSB were formed on sterile 12-well plates via the same approach outlined in “Development of WSB and DSB,” above. The DSBs were rinsed twice with DI water to remove any unattached cells before adding 1 mL of different flavonoid solutions to each well, incubated for 1 min, followed by addition of 1 mL of buffered peptone to neutralize the sanitizing action. Finally, each well was drained, dyed with the LIVE/DEAD viability kit, and measured by a fluorescence microplate reader with an excitation wavelength of 485 nm and fluorescence intensity emission wavelengths of 530 (green cells) and 630 (red cells) nm.

Morin was dissolved in 70% IPA to create a concentration gradient with final concentrations of 10, 100, 1,000, and 10,000 $\mu\text{g}/\text{mL}$. The approach for TEM imaging, CV staining, and enumeration after a 1-min morin treatment was performed according to that described above in “Evaluation of sanitizer tolerance between WSB and DSB” and “Electron microscopy imaging of WSB and DSB,” respectively.

The leakage of nucleic acids and proteins from the cytoplasm was assessed via an approach published in Qian et al. (31). The planktonic *Salmonella* sample was obtained by resuspending the cell pellets from “Bacterial strains and culture conditions,” above, in 10 mL of 0.1% PW. A total of 10 mL of bacterial suspension was mixed with DI water (control), 70% IPA, and 100 $\mu\text{g}/\text{mL}$ morin at a 1:1 ratio for 1 min before centrifugation of $10,000 \times g$ at 4°C for 15 min. The supernatants were immediately collected and transferred to a quartz cuvette for optical measurements of nucleic acids (260 nm) and proteins (280 nm).

Statistical analysis

Each experiment was conducted individually in triplicate. The statistical data were subjected to one-way analysis of variance via the Waller–Duncan multiple range test in SPSS software (IBM, USA). Statistical significance was determined for differences with a P value of less than 0.05.

RESULTS AND DISCUSSION

Salmonella DSB development in comparison with WSB

Given that there is presently no standard technique for DSB generation in food microbiology, we used the Centers for Disease Control biofilm model with some

modifications (17). Unlike WSB formation, which is simply adding bacterial suspension to the surface and allowing cell attachment and biofilm development, this protocol includes cycles of hydration and dehydration of biofilms (Fig. 1A), which simulate the periodic dryness or wetness in the food processing environment. CLSM was utilized to track the bacterial changes during WSB and DSB development, and the samples were stained with a Live/Dead BacLight viability kit. This commercial kit consists of two stains, SYTO9 and propidium iodide (PI), both of which stain nucleic acids. SYTO9 is able to diffuse across the intact cell membrane of live cells, emitting a green fluorescence signal, whereas PI enters only cells with damaged cytoplasmic membranes, with a red fluorescence signal (32). Microscopy images were taken at each step of the biofilm protocol (Fig. 1A), and the green and red cell signals were further analyzed via BiofilmQ (Fig. 1B).

During the first 48 h, both WSB and DSB were treated to similar conditions and hydrated with a 5% TSB solution. The bulk of the cells in both biofilms emitted green signals, whereas a minor proportion of the cells produced red signals. Following that, the WSB stayed hydrated for another 48 h, but the DSB was subjected to air dry and remained dehydrated over the following 48 h. Because of the nutritional depletion in 5% TSB, WSB showed a drop in total cell signals. On the other hand, there was a noticeable change from green to red cells in the DSB, showing that desiccation stress reduced membrane permeability. Previous research has shown that desiccation induces the condensation of cellular molecules, resulting in the reduction of the hydration shell around proteins. This process contributes to the conformational changes of protein, causing denaturation and the loss of enzymatic activity. Due to the inactivation of antioxidant enzymes, free radicals are accumulated inside the cell, causing damage to the cellular membrane (33). After adding 5% TSB to both WSB and DSB for 6 h, nutritional supplementation led to a substantial doubling of total cell signals in both biofilms ($P < 0.05$). Notably, the percentage of green cells dropped while the proportion of red cells grew in the WSB, but the DSB showed the reverse tendency in terms of green and red cells. The last round of hydration and dehydration in WSB and DSB, respectively, lasted 66 h. The green and red cell proportions in WSB remained stable despite a drop in overall cell signal. However, with the DSB, the loss in the overall cell signal was less apparent, with the green percentage falling and the red proportion rising considerably ($P < 0.05$).

Macroscopic analysis of *Salmonella* DSB in comparison with WSB

With the use of the plating method, the initial *Salmonella* cell population of WSB was significantly greater than that of DSB ($P < 0.05$, Fig. 2A). However, our previous total cell signals measured by the Live/Dead BacLight viability kit revealed the opposite trend (Fig. 1B), suggesting that a significant portion of the bacteria in the DSB were in the viable but nonculture (VBNC) state, which could be induced by desiccation stress and starvation. While instances of bacteria reaching VBNC states under hostile conditions have been extensively documented (34, 35), the molecular mechanisms underlying the VBNC state is still not fully understood. Research has indicated that in the VBNC state, rod-shaped microorganisms like *E. coli* and *Salmonella* can transform into a coccoid morphology (36), which is linked to significant alterations in cell wall constituents, including the peptidoglycan crosslinks, glycan chains, cytoplasmic membrane, lipoproteins, and fatty acid composition (37). These alterations enhance the stability of the cell wall and membrane in VBNC cells, hence conferring resistance to desiccation.

CV staining was subsequently used to measure EPS production since it represents a major shield for bacterial protection (18). The results are shown in Fig. 2B; DSB consisted of much more biomass than WSB ($P < 0.05$). Considering that research on DSB in the food industry is a nascent area of study, understanding of EPS generation in DSB is constrained, and the mechanisms behind DSB biomass production remain inadequately clarified. Nonetheless, numerous investigations have shown that EPS biosynthesis was upregulated in various microorganisms subjected to desiccation (38, 39). EPS may protect bacteria against desiccation via many mechanisms (40). For instance, EPS

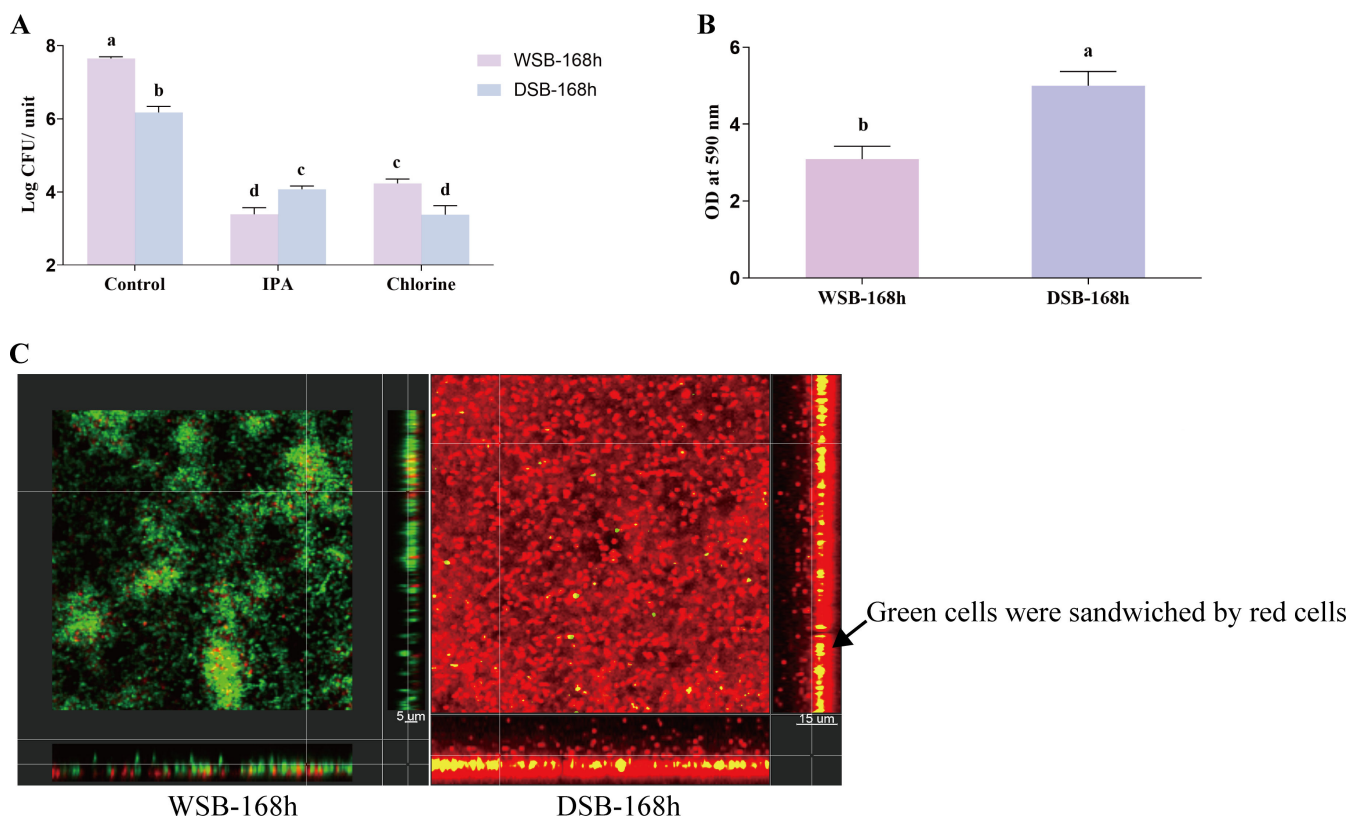


FIG 2 Enumeration of *S. Typhimurium* WSB and DSB upon various treatments (A), EPS production of *S. Typhimurium* WSB and DSB (B), and CLSM section views of *S. Typhimurium* WSB and DSB (C). Means \pm standard deviations ($n = 3$) are used to present the data. Means with different letters indicate a significant difference ($P < 0.05$).

has hygroscopic properties, enabling it to retain water for extended durations. Low permeability may diminish water loss from the cell during fast desiccation and inhibit the ingress of hazardous chemicals into the cell. EPS is also anticipated to possess the capability to make biological glass; however, this has not yet been empirically verified.

Finally, Fig. 2C shows CLSM images of the WSB and DSB. The CLSM pictures depict three parts of the biofilm. The outer layer of the biofilm is shown on the top left, and two cross-section photos of the biofilm can be seen on the right and bottom. Green and red cells were homogeneously scattered vertically in the WSB, which was about 5 μm thick, and DSB had a heterogeneous vertical distribution with a thickness of 15 μm . The exterior layer of DSB is mostly covered by red cells, with green cells inserted between the red cells, appearing yellow in the picture. Though the mechanism of this “sandwich” structure of DSB remains unclear, the outermost layer of cells may experience the most severe desiccation damage, resulting in membrane impairment, then turn red. Conversely, the innermost layer of cells may get advantages from the outer cells, which behave similarly to EPS in retaining moisture and reducing water loss, so experiencing less desiccation and maintaining a green appearance. Likewise, these inner green cells may benefit from the sandwich structure of DSB upon antimicrobials, since the outer red cells would serve as a protective barrier for the inner green cells when the antimicrobials reach the biofilm.

In accordance with these findings, 70% IPA and 200- $\mu\text{g}/\text{mL}$ chlorine, which are routinely used for food surface sanitization, were chosen as waterless and water-based sanitizers, respectively, and their antibacterial properties were tested against WSB and DSB. Indeed, WSB consistently showed a greater decrease after both sanitization treatments ($P < 0.05$, Fig. 2A). IPA reduced WSB and DSB by 4.26 ± 0.19 and $1.55 \pm$

0.13 log CFU/sample, respectively, and chlorine reduced them by 3.42 ± 0.20 and 2.80 ± 0.30 log CFU/sample, respectively.

Microscopic analysis of *Salmonella* DSB in comparison with WSB

Figure 3 shows the morphological distinctions between WSB and DSB via SEM and TEM. In general, *Salmonella* WSB exhibited an extremely heterogeneous distribution of scattered cell clusters, whereas DSB cells were evenly dispersed on the surface. Although there is a scarcity of research on the characteristics of DSB, the absence of fluid may be one of the potential explanations for their unique structure. In contrast to the WSB community, where bacteria can readily flow and gather closely for nutrient exchange or cooperation (41), bacterial movement in DSB is restricted, and bacteria are compelled to survive *in situ*. Additionally, the structure of filamentous EPS was commonly observed in WSB but not in DSB, as the SEM had a higher magnification. Similar characteristics were also identified in other WSB investigations (42–44). Finally, the interior structure of the individual cell between the WSB and DSB was examined via TEM. The images of WSB cells revealed a distinct plasma membrane and outer membrane, which were separated by the periplasm. Conversely, the DSB cells were enclosed by dense capsules, which was not unexpected, given that capsules could assist in the preservation of water within the cell to prevent desiccation, and numerous studies have documented the increased production of capsular polysaccharides when microorganisms are subjected to desiccation stress (45–47).

DSB single-cell landscape and heterogeneity of functional clusters

According to the preceding discussion in “*Salmonella* DSB development in comparison with WSB,” there was a continuous shift in the percentage of green and red cells throughout the development of DSB, indicating that dramatic changes in cell status occurred continuously within the DSB, with cells adapting or not adapting to desiccation. This prompted us to question the reasons for such individual heterogeneity among biofilm cells. Thus, we applied single-cell microbiological methods to analyze the transcriptomics of *Salmonella* DSB and identify functional clusters (Fig. 4). Overall, over

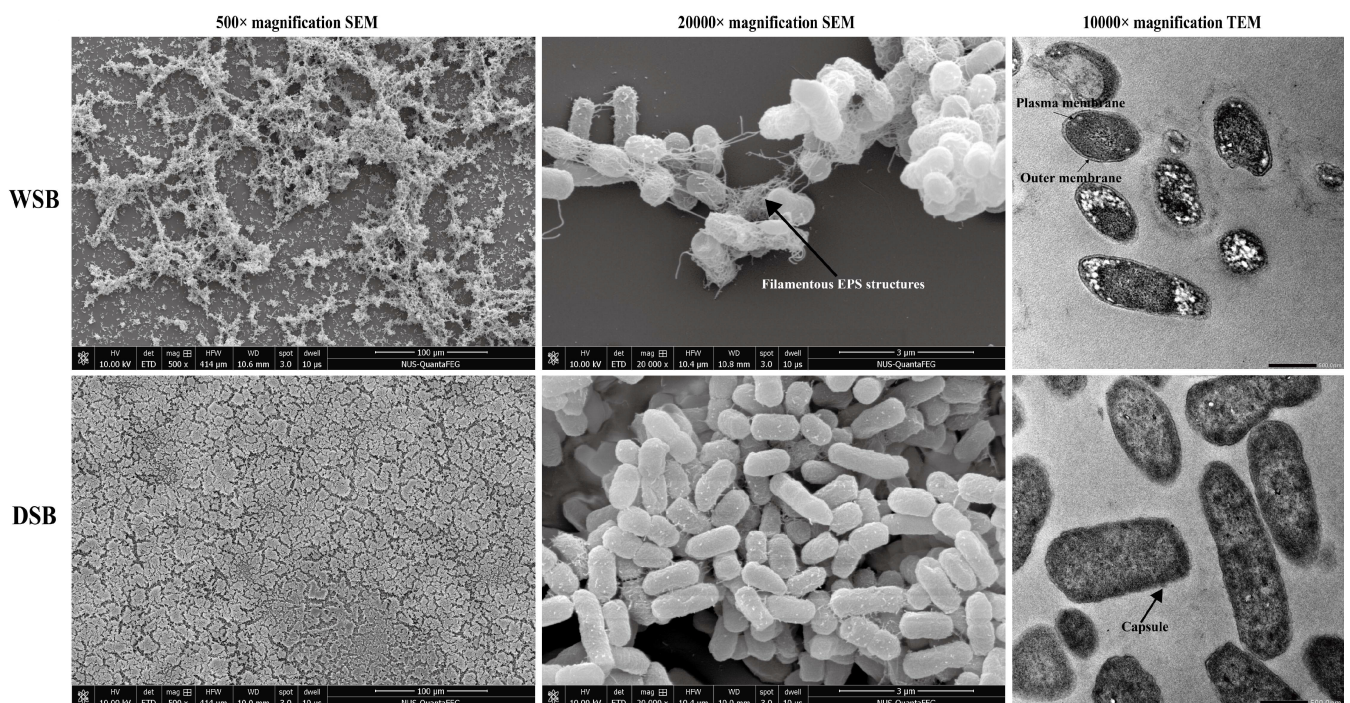


FIG 3 Representative SEM and TEM images of *S. Typhimurium* WSB and DSB.

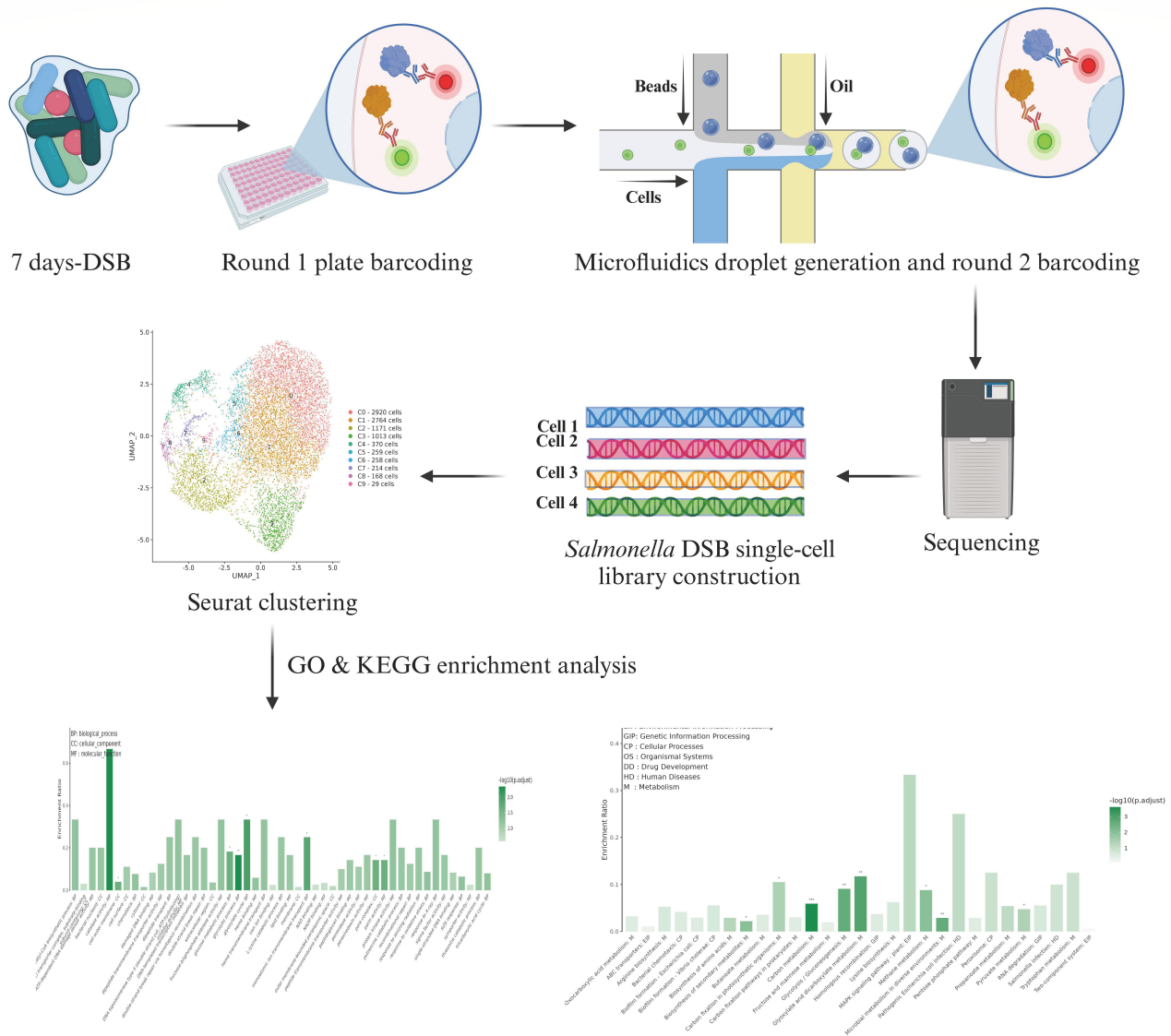


FIG 4 Overall process for single-cell transcriptomics. This workflow involves microbial single-cell sequencing of DSB (22), single-cell transcriptome annotation, and functional cluster identification and interpretation. Figure created with BioRender.com.

9,000 DSB cells were successfully obtained via a droplet-based single-microbe technique. The quality control results are presented in Fig. S1A and B, with an average number of reads per cell of 696. The UMI plot clearly revealed that the lowest UMI of a validated cell was approximately 130 (Fig. S1A). Additionally, the UMI distribution diagram (Fig. S1B) reveals that the general number of UMIs in all clusters is greater than 100, indicating that these cell clusters are not invalid or dead cells.

A clustering analysis with batch effect correction was conducted on all 9,231 cells following normalization and a succession of benchmarking (Fig. 5A). Ten clusters were identified. The top three DEGs in each cluster (ranked by average log2FC value) are identified and visualized in Fig. 5B, and the distribution of the top one DEG from each cluster on the UMAP plot is also highlighted in Fig. 5C. Finally, the functional annotation result of each cluster was determined by the most significant term based on P_{adjust} in the GO enrichment analysis (Table S3) and is presented in Fig. 5D. For example, cluster 2 is designated the catalase activity functional cluster since the most prominent GO term (with the smallest P_{adjust}) is catalase activity. Additionally, the STM14-RS09555

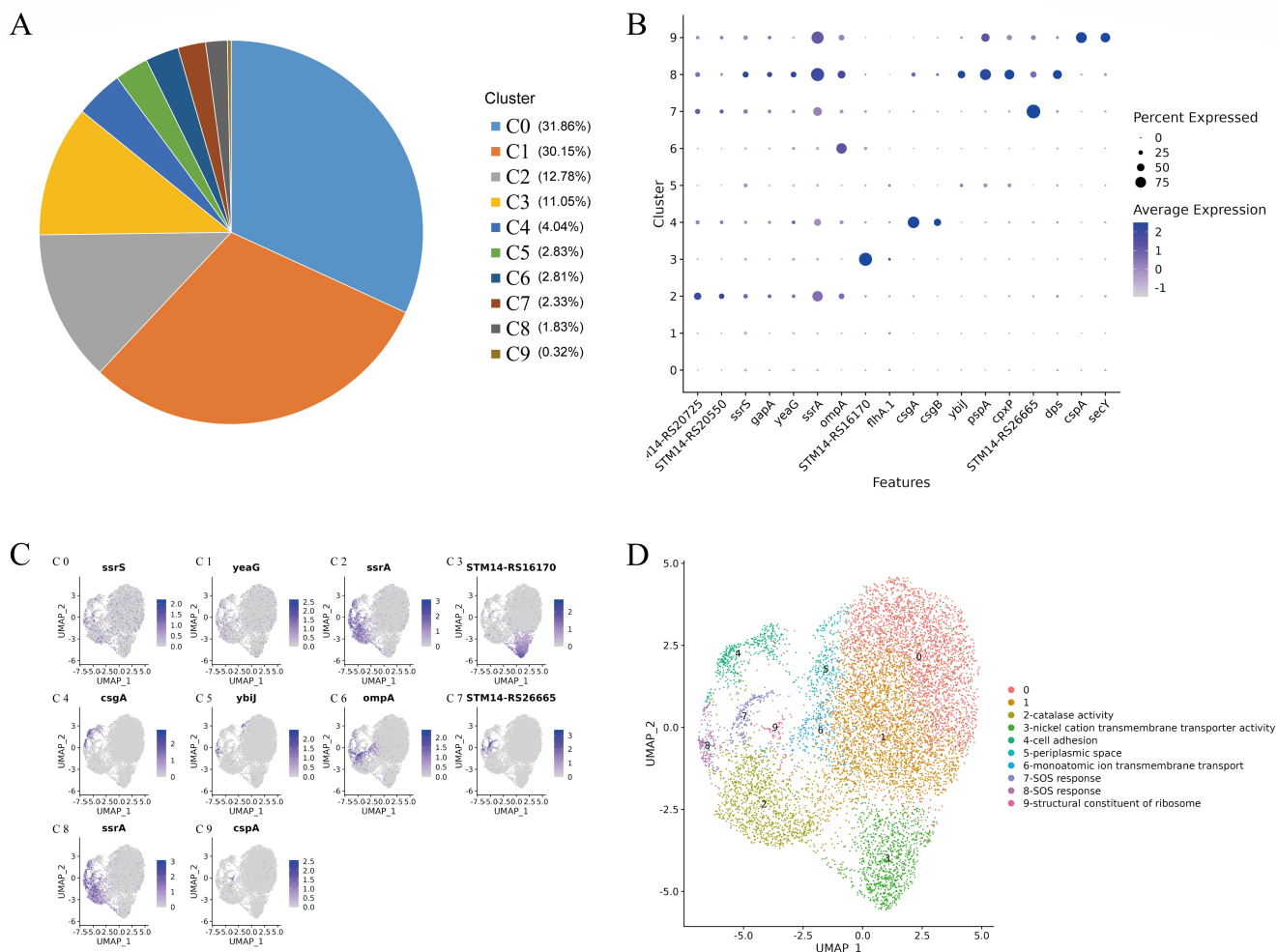


FIG 5 (A) Pie chart of the proportion of cells in each cluster. (B) Dot plot showing the expression of the top three genes that are significantly different among clusters and the percentage of cells expressing these genes in each cluster. The distribution of the top DEGs from each cluster is highlighted on UMAP. (C) The purple bars represent the normalized expression of a gene across all cells analyzed. (D) The UMAP plot for 10 functional clusters identified from *Salmonella* dry surface biofilm cells. DEG, differentially expressed gene; UMAP, uniform manifold approximation and projection.

and *katE* genes (Table S2), which encode the catalase enzyme associated with reactive oxygen species (ROS) removal, are specifically expressed by cells in this cluster (48). These findings indicate that this functional cluster has metabolic activity. Concurrently, the proportion of these two genes in this cluster was relatively high in comparison to that in the other clusters (Table S2). Consequently, we designated this functional cluster catalase activity (other functional clusters were also named similarly, as detailed in Table S3). Overall, at the single-cell RNA level, *Salmonella* DSB cells can be categorized into eight different functional clusters.

Clusters 0 and 1 accounted for more than half of the identified cells, whereas these two clusters did not receive annotations, indicating that no genes were significantly expressed within these two clusters compared with the other clusters. Given that the quality control results (Fig. S1) confirmed that all sample cells were alive, it seems reasonable to assume that the majority of *Salmonella* cells were metabolically inactive during DSB development. Unsurprisingly, multiple studies have shown that bacteria may enter a state of metabolic dormancy, which serves as an important survival strategy for nonsporulating bacteria to withstand desiccation. The transition to a VBNC state has been documented in several bacteria, including pathogenic strains such as *Acinetobacter baumannii*, *Escherichia coli*, and *S. enterica* (33, 49). For instance, a transcriptomic study

revealed that less than 5% of the genome of *S. enterica*, when cultured in peanut oil, is transcribed. In comparison, 78% of the genome is transcribed when the organism is grown in aqueous media (50). This low level of metabolic activity may play a role in the ability of bacteria to survive in low-moisture environments.

Cluster 2 genes are categorized as having catalase activity owing to the high expression of catalase-associated genes involved in the antioxidative system. It is now well recognized that oxidative stress is critical for understanding the desiccation process (51). Desiccation, for example, causes excessively high levels of ROS, including superoxide anion, hydroxyl radicals, and hydrogen peroxide, in microorganisms (40). This is most likely due to two reasons. First, desiccation can damage the entire electron transport chain and protein enzymes, which halts the ability of the cell to mitigate ROS (52). On the other hand, desiccation leads to mechanical effects such as increased intracellular concentration, cell shrinkage, and reduced cytosol fluidity and ultimately promotes the formation of ROS (40). As a result, catalase activity is critical in the defense against oxidative stress. In general, ROS is removed via superoxide dismutase, catalases, and peroxidases. Superoxide dismutase first converts superoxide anions to oxygen and hydrogen peroxide, which are then destroyed by catalases and peroxidases (53). Other investigations have consistently shown that catalase activity peaks when *Acinetobacter* is dried (54) and that deleting the catalase biosynthesis-related gene *katE* may affect its xerotolerance (54, 55). Overall, under uniform desiccation stress, DSB cells display various antioxidative abilities, with cells in cluster 2 aggressively promoting catalase activity. More importantly, continual damage to the cell membrane caused by desiccation is likely the reason that red cells are the predominant type of DSB (Fig. 1B). Cells with antioxidative capabilities, such as cluster 2, may be able to reduce ROS damage, repair their membranes, and eventually detected as green signals in CLSM images. In addition to cluster 2, both clusters 7 and 8, which are annotated as the SOS response, were also found to be associated with oxidation defense. The SOS response is crucial for the repair of damaged DNA (56). Desiccation-induced ROS can lead to DNA damage in bacteria, triggering the activation of the SOS repair mechanism to preserve the integrity of the bacterial genome. As a result, the activation of the SOS response in a cell may lead to the acquisition of random adaptive mutations in its genome. These mutations are then chosen and permanently established in the microbial population because of the SOS repair mechanism (57). Later, the adopted cell may persist in dry environments. In accordance with our clustering study, clusters 2, 7, and 8 exhibited close proximity to each other in the UMAP plot (Fig. 5D). These findings indicate that their gene expression may have a shared function in defending against oxidative damage caused by desiccation.

Cluster 3 is annotated as having nickel cation transmembrane transporter activity. For certain pathogen virulence factors, nickel is a necessary element. Pathogens must transport metals effectively because of their scarcity in hosts and balance metal toxicity concerns with the development of pathogenic virulence (58). Urease and Ni-enzyme hydrogenases are the two most significant virulence-associated components (59), and studies have shown that *Salmonella* Typhimurium has three different Ni-enzymes, all of which are associated with virulence (60). Despite cluster 4 being far from cluster 3 on the UMAP plot (Fig. 5D), cluster 4 is annotated as cell adhesion, which has long been recognized as a significant factor in pathogenic virulence (61). For many bacterial pathogens that rely on infection to cause disease, attachment to host surfaces is a critical step in pathogenesis (62). Several instances of pathogens have lost their ability to adhere to surfaces. As a result, these pathogens have become harmless and may even have beneficial effects on the host (63, 64). Similarly, clusters 5 and 6 are also associated with *Salmonella* virulence. Although cluster 5 is classified as a periplasmic space because it has the highest P_{adjust} value in the GO annotation, the second most important GO annotation is thiosulfate sulfurtransferase activity, with the *pspE* gene being enriched in both GO terms. PspE, a phage-shock protein from the glycerol 3-phosphate regulon of *S. Typhimurium*, was found to be a thiosulfate sulfurtransferase (65). Wallrodt et al. (66)

demonstrated that the thiosulfate sulfurtransferase PspE contributes to *S. Typhimurium* pathogenicity in a mouse model of systemic illness. Finally, cluster 6 was annotated as monoatomic ion transmembrane transport, with the *ompA* gene being enriched. OmpA proteins have crucial functions in pathogenesis, such as facilitating bacterial adhesion and infection, escaping the host immune system, and stimulating proinflammatory cytokine production (67). Interestingly, Chowdhury et al. (68) recently revealed that the outer membrane protein OmpA may shield bacteria from harsh conditions by preserving the integrity of their outer membranes, which may also contribute to the shift between green and red cells during DSB formation. Overall, the presence of many clusters of DSB cells related to virulence activity clearly indicates that *Salmonella* DSB cells represent a significant risk to food safety. This could contradict the conventional belief that dehydrated cells, which are metabolically dormant, may be less hazardous.

Cluster 9 (the structural part of the ribosome) contained the lowest number of examined cells. However, among the enriched genes associated with this GO term, *cspA* was predominantly expressed in this cluster (Table S2). More precisely, *cspA* represents 75.9% of the genes expressed in all cells belonging to cluster 9, but it represents only 1.4% of the genes expressed in all cells not belonging to cluster 9. This finding indicates that *cspA* is the distinctive gene in cluster 9. The CspA protein, a prominent cold-shock protein in *E. coli*, functions as an RNA chaperone. It was originally believed that its role was to increase translation at low temperatures by disrupting mRNA structures. Kim and Wood (69) reported that CspD, a member of the CspA family, is involved in the development of persistent cells in *E. coli*. Furthermore, recent research has shown that the buildup of the CspA protein may contribute to the development of persisters in *Enterococcus faecium* (70). Overall, while accounting for the lowest part of the DSB population, cluster 9 might be prominently implicated in the development of persistent cells.

Overall, the results from the DSB single-cell analysis clearly revealed that although the majority of *Salmonella* cells enter the dormant state and become metabolically inactive, a certain number of bacteria can resist desiccation damage via either antioxidation enhancement or DNA damage repair. In addition, a group of *Salmonella* cells can actively express virulence factors even under dry conditions. Unlike conventional transcriptomics studies of desiccated *Salmonella* (71–73), which assess average gene expressions across a substantial cell population, this study applied single-cell transcriptomics to quantify the transcriptomes of individual cells, thereby highlighting intrabiofilm heterogeneity with unparalleled resolution. Thanks to this high sensitivity, enriched pathways in DNA protection, antioxidation, or ribosome activities were successfully identified in this study, while these notable changes might be obscured by the overwhelming presence of extraneous sequencing data in other research. For instance, contrary to our findings, Abdelhamid and Yousef (74) applied conventional transcriptomics on desiccated *Salmonella* and discovered that the expression of virulence genes was inactive upon desiccation. Despite the potential influence of numerous factors (e.g., bacterial strain, experimental settings, and food matrix) on the transcriptomics results, in our case, the majority of desiccated cells are metabolically indeed dormant. Therefore, it is unsurprising that the global transcriptomics screening may overlook certain genes that have only been significantly altered in a minor group of cells.

Evaluation of flavonoids as waterless sanitizers against *Salmonella* DSB

In dry food processing environments, particularly for the LMF industry, incorporating water into cleaning and sanitization methods to prevent any moisture for pathogens and microbial growth is common but also leads to DSB emergence (9). As a result, biofilm eradication via dry sanitization is critical for preventing product or residue exposure to moisture. Alcohol-based sanitizers are the most often used waterless disinfectants in the LMF industry, but our investigation revealed that 70% IPA has poor effectiveness against DSB. Thus, a list of 39 flavonoids dissolved in 70% IPA was screened for their collective efficiency against *Salmonella* DSB, and the results are shown in Fig. 6B. Overall,

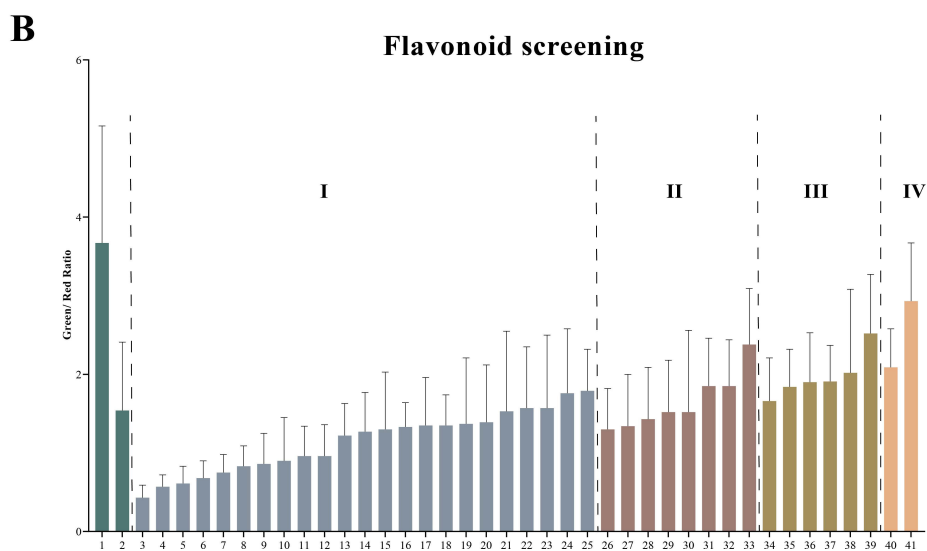
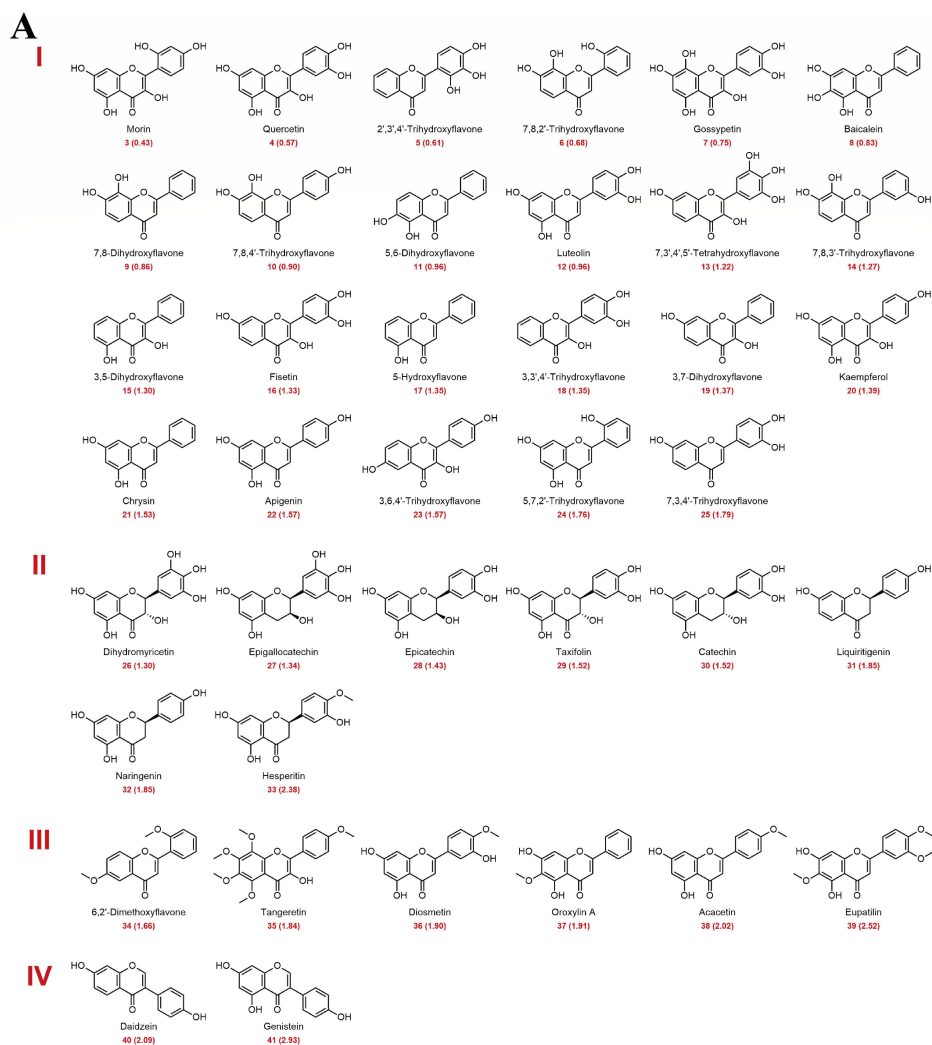


FIG 6 The structure of 39 flavonoids tested against *S. Typhimurium* DSB (A); the green:red ratio of *S. Typhimurium* DSB after various flavonoid treatments for 1 min (B). Note: 1 and 2 represent the DI water and IPA treatments, respectively. Means \pm standard deviations ($n = 3$) are used to present the data.

morin outperformed the other 38 flavonoids in terms of antibiofilm activity, lowering the green:red ratio from 3.67 to 0.43, and the whole list of flavonoids was categorized into four groups on the basis of structural differences in comparison to morin (Fig. 6A). Group I comprised flavones and flavanols. Variations in antimicrobial efficacy were observed for several flavonoids that were structurally similar to morin. For example, quercetin, which differs from morin in terms of the position of a hydroxyl group on the B ring (3'-carbon instead of 2'-carbon), still has relatively high antimicrobial efficacy. In contrast, kaempferol, which lacks a hydroxyl group on the 2'-carbon at the B ring, showed relatively lower antimicrobial efficacy than morin. In addition, flavonoids in group II (flavan-3-ols, flavanones), group III (flavones containing methoxy groups) and group IV (isoflavones) displayed relatively lower antimicrobial efficacy than morin. As our study focused on the evaluation of an effective flavonoid to eradicate DSB, morin was chosen to further investigate its antimicrobial mechanism against DSB.

The antimicrobial efficacy of morin was optimized by evaluating it with a concentration gradient (10, 100, 1,000, and 10,000 $\mu\text{g}/\text{mL}$) (Fig. 7A), as the manufacturer stated that the maximal solubility of morin in ethanol is 10,000 $\mu\text{g}/\text{mL}$. On the basis of our results, the efficacy of 10- $\mu\text{g}/\text{mL}$ morin (1.69 ± 0.25 log CFU/sample reduction) was comparable to that of 70% IPA alone (1.55 ± 0.20 log CFU/sample reduction) ($P > 0.05$). When the morin concentration was increased 10-fold, the efficacy was enhanced by 89.76%, resulting in a 3.21 $\mu\text{g}/\text{mL}$ log CFU/sample reduction at 100 $\mu\text{g}/\text{mL}$. Since then, the rate of increase in efficacy has slowed. From 100 to 1,000 $\mu\text{g}/\text{mL}$, the antibacterial efficacy (4.32 ± 0.24 log CFU/sample reduction) increased by 34.85%, whereas from 1,000 to 10,000 $\mu\text{g}/\text{mL}$, the antimicrobial efficacy (5.18 ± 0.16 log CFU/sample reduction) increased by 19.71%. Although the antimicrobial effectiveness of morin is enhanced by a relatively high concentration, 100 $\mu\text{g}/\text{mL}$ was chosen as the working concentration for cost-efficient reasons. Subsequently, the impact of morin (100 $\mu\text{g}/\text{mL}$) on the EPS matrix was investigated via CV staining (Fig. 7B). Morin reduced biomass from 5.00 ± 0.37 to 3.38 ± 0.17 nm (OD_{560}) ($P < 0.05$), but its efficiency was not significantly different from that of IPA alone ($P > 0.05$), indicating that IPA was primarily responsible for biomass removal rather than morin.

Changes in the morphology of DSB cells after each treatment were observed via TEM (Fig. 7C). As stated previously, DSB cells were initially covered with a dense layer of capsule, and after 70% IPA treatment, a gap was observed between the capsular and bacterial outer membranes. Bacterial capsules are mostly composed of exopolysaccharides (75), and polysaccharides of various polarities can progressively precipitate in ethanol. During precipitation, small-molecular-weight sugar components may be detached due to their strong alcohol compatibility, causing a reduction in the dielectric constant (76). On the other hand, upon morin treatment, not only was a clear gap observed between the capsule and outer membranes, but also the entire cytoplasm appeared empty and hollow with incomplete membranes. Studies have shown that morin can disrupt the membrane structure, leading to lipid disorientation and intracellular leakage (77, 78). Therefore, to verify the effects of IPA and morin on the cellular membrane, the release of nucleic acids and proteins from *Salmonella* planktonic cells was examined (Fig. 7D). Following 70% IPA treatment, there was little protein leakage ($P < 0.05$) but no significant leakage of nucleic acids ($P > 0.05$). On the other hand, three times more nucleic acid and protein leakage was caused by morin than by IPA alone.

Taken together (Fig. 7A through D), it is reasonable to conclude that the tolerance of the DSB to different sanitizers was enhanced at the individual cell level by thick capsule encapsulation. Although the antibacterial activity of IPA against DSB is limited, its primary role is to detach the capsule from the DSB, allowing morin to breach the capsular protection and cause damage to bacterial membranes.

Conclusions

So far, dealing with DSB has been a concern in the food sector, particularly in LMF processing facilities where DSB occurs often. This research examined the properties of

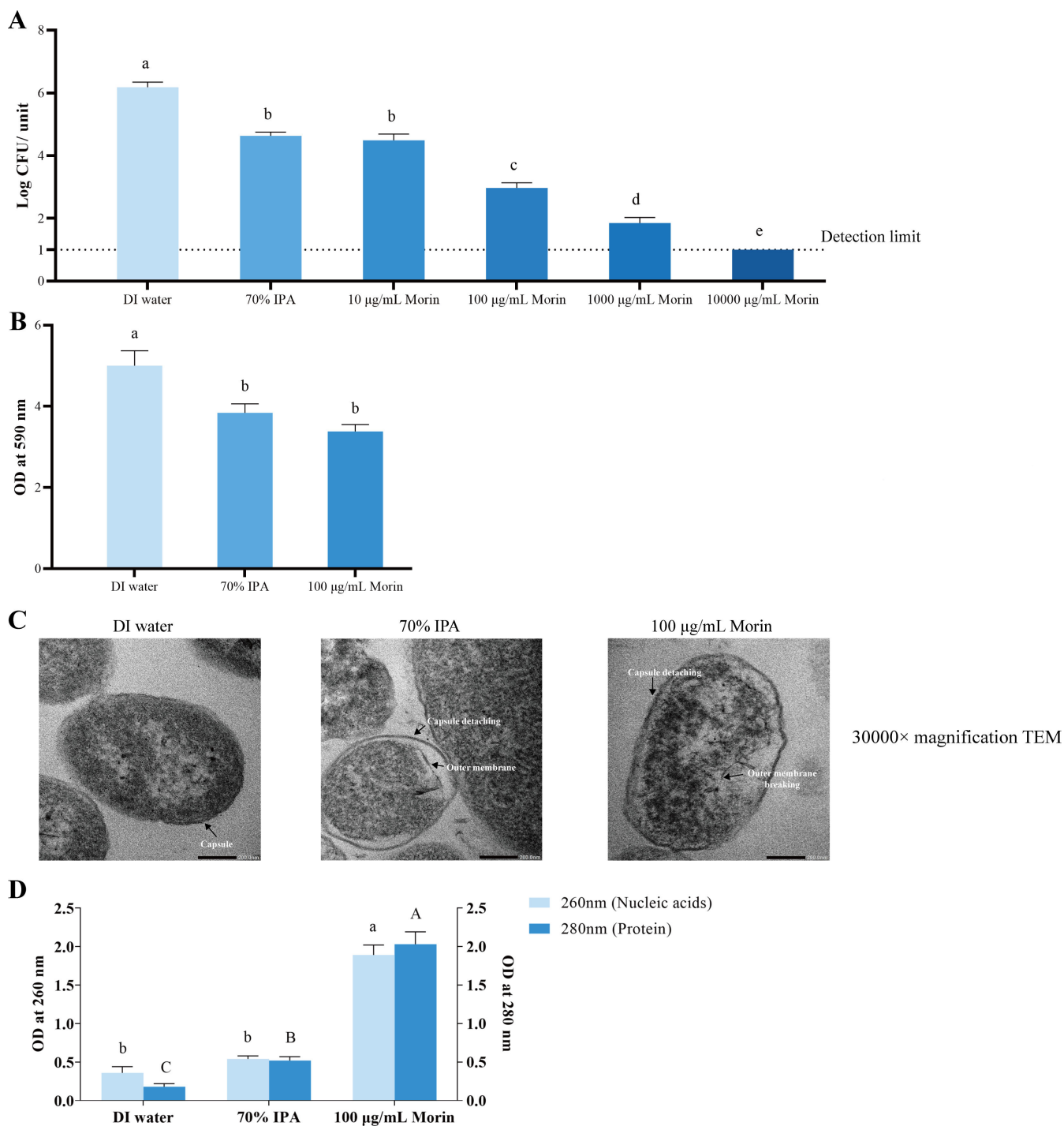


FIG 7 Concentration gradient test of morin on *S. Typhimurium* DSB (A), EPS profiles of *S. Typhimurium* DSB upon various treatments (B), TEM images of *S. Typhimurium* DSB upon various treatments (C), and changes in the leakage of nucleic acid and protein within *S. Typhimurium* DSB upon various treatments (D). Means ± standard deviations ($n = 3$) are used to present the data. The means with different letters indicate a significant difference ($P < 0.05$).

DSB formed by *Salmonella*, including their growth patterns, sanitizer tolerance, biofilm morphology, and single-cell landscape. Overall, DSB demonstrated stronger sanitizing tolerance than WSB, most likely due to the sandwich structural protection. The single-cell transcriptomics highlights the functional variability that occurs within the DSB community, with some populations exhibiting enhanced antioxidative capabilities and active virulence factors that may represent a hazard to food safety. Morin formulated with 70%

IPA was shown to be efficient against *Salmonella* DSB, indicating a high potential in the LMF business, where the majority of sanitization must be accomplished without the use of water. In the future, assessment of morin-based sanitizers against dry biofilm in genuine food processing environments is necessary, as the varying microbial microflora composition in the biofilm and food residuals may affect its antimicrobial effectiveness.

ACKNOWLEDGMENTS

We thank the Electron Microscopy Unit (<https://medicine.nus.edu.sg/core-facilities/electron-microscopy-unit-emu/>) at the National University of Singapore and the team, particularly Ms. Micky Leong, for their support and assistance in the electron microscopy work. We also thank Shu Ying Lee from the Confocal Microscopy Unit at the Yong Loo Lin School of Medicine for the confocal laser scanning microscopy work.

This research was financed by a department fund at the Department of Food Science and Technology, National University of Singapore (E-160-00-0015-01, Food Microbial Safety Research, to D.L.) and National University of Singapore (Suzhou) Research Institute (Key Technology Research and Industrialization of Food for Special Medical Use and Future Foods, to D.L. and D.H.).

AUTHOR AFFILIATIONS

¹Department of Food Science and Technology, National University of Singapore, Singapore

²National University of Singapore (Suzhou) Research Institute, Suzhou, China

³School of Health Science and Engineering, University of Shanghai for Science and Technology, Shanghai, China

AUTHOR ORCID*s*

Zeja Lin  <http://orcid.org/0000-0002-4196-9243>

Dan Li  <http://orcid.org/0000-0001-6645-2489>

FUNDING

Funder	Grant(s)	Author(s)
NUS Faculty of Science, National University of Singapore (NUS, FoS)	Food Microbial Safety Research	Dan Li
NUS Suzhou Research institute	Key Technology Research and Industrialization of Food for Special Medical Use Future Foods	Dan Li

AUTHOR CONTRIBUTIONS

Zeja Lin, Conceptualization, Data curation, Investigation, Methodology, Writing – original draft | Zhiqian Liang, Investigation, Methodology | Shuang He, Investigation, Methodology | Fion Wei Lin Chin, Resources | Dejian Huang, Resources, Supervision | Yi Hong, Investigation | Xiang Wang, Resources, Supervision | Dan Li, Conceptualization, Funding acquisition, Project administration, Supervision, Validation, Writing – review and editing

ADDITIONAL FILES

The following material is available [online](#).

Supplemental Material

Figure S1 (AEM01623-24-s0001.docx). Quality control results of single-cell transcriptomics.

Tables S1 to S3 (AEM01623-24-s0002.xlsx). Single-cell RNAseq setup and data.

REFERENCES

- Ehuwa O, Jaiswal AK, Jaiswal S. 2021. *Salmonella*, food safety and food handling practices. *Foods* 10:907. <https://doi.org/10.3390/foods10050907>
- Karuppuchamy V, Heldman DR, Snyder AB. 2024. A review of food safety in low-moisture foods with current and potential dry-cleaning methods. *J Food Sci* 89:793–810. <https://doi.org/10.1111/1750-3841.16920>
- Russo ET, Biggerstaff G, Hoekstra RM, Meyer S, Patel N, Miller B, Quick R, Salmonella Agona Outbreak Investigation Team. 2013. A recurrent, multistate outbreak of *Salmonella* serotype Agona infections associated with dry, unsweetened cereal consumption, United States, 2008. *J Food Prot* 76:227–230. <https://doi.org/10.4315/0362-028X.JFP-12-209>
- Han R, Klu YAK, Chen J. 2017. Attachment and biofilm formation by selected strains of *Salmonella enterica* and enterohemorrhagic *Escherichia coli* of fresh produce origin. *J Food Sci* 82:1461–1466. <https://doi.org/10.1111/1750-3841.13722>
- Villa-Rojas R, Zhu M-J, Paul NC, Gray P, Xu J, Shah DH, Tang J. 2017. Biofilm forming *Salmonella* strains exhibit enhanced thermal resistance in wheat flour. *Food Control* 73:689–695. <https://doi.org/10.1016/j.foodcont.2016.09.021>
- von Hertwig AM, Prestes FS, Nascimento MS. 2022. Biofilm formation and resistance to sanitizers by *Salmonella* spp. isolated from the peanut supply chain. *Food Res Int* 152:110882. <https://doi.org/10.1016/j.foodres.2021.110882>
- Morasi RM, Rall VLM, Dantas STA, Alonso VPP, Silva NCC. 2022. *Salmonella* spp. in low water activity food: occurrence, survival mechanisms, and thermoresistance. *J Food Sci* 87:2310–2323. <https://doi.org/10.1111/1750-3841.16152>
- Steenackers H, Hermans K, Vanderleyden J, De Keersmaecker SCJ. 2012. *Salmonella* biofilms: an overview on occurrence, structure, regulation and eradication. *Food Res Int* 45:502–531. <https://doi.org/10.1016/j.foodres.2011.01.038>
- Alonso VPP, Gonçalves MPMBB, de Brito FAE, Barboza GR, Rocha L de O, Silva NCC. 2023. Dry surface biofilms in the food processing industry: an overview on surface characteristics, adhesion and biofilm formation, detection of biofilms, and dry sanitization methods. *Compr Rev Food Sci Food Saf* 22:688–713. <https://doi.org/10.1111/1541-4337.13089>
- Tewes TJ, Centeleghe I, Maillard J-Y, Platte F, Bockmühl DP. 2022. Raman microscopic analysis of dry-surface biofilms on clinically relevant materials. *Microorganisms* 10:1369. <https://doi.org/10.3390/microorganisms10071369>
- Orevi T, Kashtan N. 2021. Life in a droplet: microbial ecology in microscopic surface wetness. *Front Microbiol* 12:655459. <https://doi.org/10.3389/fmicb.2021.655459>
- Nair MS, Upadhyaya I, Amalaradjou MAR, Venkitanarayanan K. 2016. Antimicrobial food additives and disinfectants: mode of action and microbial resistance mechanisms, p 275–301. In *Foodborne pathogens and antibiotic resistance*
- Harada AMM, Nascimento MS. 2021. Effect of dry sanitizing methods on *Bacillus cereus* biofilm. *Braz J Microbiol* 52:919–926. <https://doi.org/10.1007/s42770-021-00451-0>
- Kim YK, Roy PK, Ashrafudoulla M, Nahar S, Toushik SH, Hossain MI, Mizan MFR, Park SH, Ha S-D. 2022. Antibiofilm effects of quercetin against *Salmonella enterica* biofilm formation and virulence, stress response, and quorum-sensing gene expression. *Food Control* 137:108964. <https://doi.org/10.1016/j.foodcont.2022.108964>
- Pruteanu M, Hernández Lobato JI, Stach T, Hengge R. 2020. Common plant flavonoids prevent the assembly of amyloid curli fibres and can interfere with bacterial biofilm formation. *Environ Microbiol* 22:5280–5299. <https://doi.org/10.1111/1462-2920.15216>
- Vikram A, Jayaprakasha GK, Jesudhasan PR, Pillai SD, Patil BS. 2010. Suppression of bacterial cell-cell signalling, biofilm formation and type III secretion system by citrus flavonoids. *J Appl Microbiol* 109:515–527. <https://doi.org/10.1111/j.1365-2672.2010.04677.x>
- Amaze N, Akinbobola A, Chukwuemeka V, Abalkhaila A, Ramage G, Kean R, Staines H, Williams C, Mackay W. 2020. Development of a high throughput and low cost model for the study of semi-dry biofilms. *Biofouling* 36:403–415. <https://doi.org/10.1080/08927014.2020.1766030>
- Lin Z, Chen T, Zhou L, Yang H. 2022. Effect of chlorine sanitizer on metabolic responses of *Escherichia coli* biofilms “big six” during cross-contamination from abiotic surface to sponge cake. *Food Res Int* 157:111361. <https://doi.org/10.1016/j.foodres.2022.111361>
- Kamimura R, Kanematsu H, Ogawa A, Kogo T, Miura H, Kawai R, Hirai N, Kato T, Yoshitake M, Barry DM. 2022. Quantitative analyses of biofilm by using crystal violet staining and optical reflection. *Mat Basel* 15:6727. <https://doi.org/10.3390/ma15196727>
- Santana BP, Nedel F, Perelló Ferrúa C, Marques e Silva R, da Silva AF, Demarco FF, Lenin Villarreal Carreño N. 2015. Comparing different methods to fix and to dehydrate cells on alginate hydrogel scaffolds using scanning electron microscopy. *Microsc Res Tech* 78:553–561. <https://doi.org/10.1002/jemt.22508>
- Stirling JW. 2013. General tissue preparation methods, p 341–352. In *Diagnostic electron microscopy—a practical guide to interpretation and technique*. Wiley Publication, Sussex.
- Jia M, Zhu S, Xue M-Y, Chen H, Xu J, Song M, Tang Y, Liu X, Tao Y, Zhang T, Liu J-X, Wang Y, Sun H-Z. 2024. Single-cell transcriptomics across 2,534 microbial species reveals functional heterogeneity in the rumen microbiome. *Nat Microbiol* 9:1884–1898. <https://doi.org/10.1038/s41564-024-01723-9>
- Le DT, Durham JN, Smith KN, Wang H, Bartlett BR, Aulakh LK, Lu S, Kemberling H, Wilt C, Luber BS, et al. 2017. Mismatch repair deficiency predicts response of solid tumors to PD-1 blockade. *Science* 357:409–413. <https://doi.org/10.1126/science.aan6733>
- Satija R, Farrell JA, Gennert D, Schier AF, Regev A. 2015. Spatial reconstruction of single-cell gene expression data. *Nat Biotechnol* 33:495–502. <https://doi.org/10.1038/nbt.3192>
- Stuart T, Butler A, Hoffman P, Hafemeister C, Papalexi E, Mauck WM, Hao Y, Steockius M, Smibert P, Satija R. 2019. Comprehensive integration of single-cell data. *Cell* 177:1888–1902. <https://doi.org/10.1016/j.cell.2019.05.031>
- Becht E, McInnes L, Healy J, Dutertre C-A, Kwok IWH, Ng LG, Ginhoux F, Newell EW. 2019. Dimensionality reduction for visualizing single-cell data using UMAP. *Nat Biotechnol* 37:38–44. <https://doi.org/10.1038/nbt.4314>
- Blondel VD, Guillaume J-L, Lambiotte R, Lefebvre E. 2008. Fast unfolding of communities in large networks. *J Stat Mech* 2008:10008. <https://doi.org/10.1088/1742-5468/2008/10/P10008>
- Zhang Z, Luo D, Zhong X, Choi JH, Ma Y, Wang S, Mahrt E, Guo W, Stawiski EW, Modrusan Z, Seshagiri S, Kapur P, Hon GC, Brugarolas J, Wang T. 2019. SCINA: a semi-supervised subtyping algorithm of single cells and bulk samples. *Genes (Basel)* 10:531. <https://doi.org/10.3390/genes10070531>
- Gantenbein B, Croft AS, Larraillet M. 2020. Mammalian cell viability methods in 3D scaffolds for tissue engineering, p 1–25. In *Fluorescence methods for investigation of living cells and microorganisms*
- Stiefel P, Schmidt-Emrich S, Maniura-Weber K, Ren Q. 2015. Critical aspects of using bacterial cell viability assays with the fluorophores SYTO9 and propidium iodide. *BMC Microbiol* 15:36. <https://doi.org/10.1186/s12866-015-0376-x>
- Qian J, Ma L, Yan W, Zhuang H, Huang M, Zhang J, Wang J. 2022. Inactivation kinetics and cell envelope damages of foodborne pathogens *Listeria monocytogenes* and *Salmonella* Enteritidis treated with cold plasma. *Food Microbiol* 101:103891. <https://doi.org/10.1016/j.fm.2021.103891>

32. Gião MS, Wilks SA, Azevedo NF, Vieira MJ, Keevil CW. 2009. Validation of SYTO 9/propidium iodide uptake for rapid detection of viable but noncultivable *Legionella pneumophila*. *Microb Ecol* 58:56–62. <https://doi.org/10.1007/s00248-008-9472-x>
33. Laskowska E, Kuczyńska-Wiśnik D. 2020. New insight into the mechanisms protecting bacteria during desiccation. *Curr Genet* 66:313–318. <https://doi.org/10.1007/s00294-019-01036-z>
34. Finn S, Condell O, McClure P, Amézquita A, Fanning S. 2013. Mechanisms of survival, responses and sources of *Salmonella* in low-moisture environments. *Front Microbiol* 4:331. <https://doi.org/10.3389/fmicb.2013.00331>
35. Pazos-Rojas LA, Cuellar-Sánchez A, Romero-Cerón AL, Rivera-Urbalejo A, Van Dillewijn P, Luna-Vital DA, Muñoz-Rojas J, Morales-García YE, Bustillos-Cristales MDR. 2023. The viable but non-culturable (VBNC) state, a poorly explored aspect of beneficial bacteria. *Microorganisms* 12:39. <https://doi.org/10.3390/microorganisms12010039>
36. Dong K, Pan H, Yang D, Rao L, Zhao L, Wang Y, Liao X. 2020. Induction, detection, formation, and resuscitation of viable but non-culturable state microorganisms. *Compr Rev Food Sci Food Saf* 19:149–183. <https://doi.org/10.1111/1541-4337.12513>
37. Izgördü ÖK, Darcan C, Kariptaş E. 2022. Overview of VBNC, a survival strategy for microorganisms. *3 Biotech* 12:307. <https://doi.org/10.1007/s13205-022-03371-4>
38. McKew BA, Taylor JD, McGenity TJ, Underwood GJC. 2011. Resistance and resilience of benthic biofilm communities from a temperate saltmarsh to desiccation and rewetting. *ISME J* 5:30–41. <https://doi.org/10.1038/ismej.2010.91>
39. Weaver L, Webber JB, Hickson AC, Abraham PM, Close ME. 2015. Biofilm resilience to desiccation in groundwater aquifers: a laboratory and field study. *Sci Total Environ* 514:281–289. <https://doi.org/10.1016/j.scitotenv.2014.10.031>
40. Greffe VRG, Michiels J. 2020. Desiccation-induced cell damage in bacteria and the relevance for inoculant production. *Appl Microbiol Biotechnol* 104:3757–3770. <https://doi.org/10.1007/s00253-020-10501-6>
41. Nadell CD, Drescher K, Foster KR. 2016. Spatial structure, cooperation and competition in biofilms. *Nat Rev Microbiol* 14:589–600. <https://doi.org/10.1038/nrmicro.2016.84>
42. Böhning J, Tarafder AK, Bharat TAM. 2024. The role of filamentous matrix molecules in shaping the architecture and emergent properties of bacterial biofilms. *Biochem J* 481:245–263. <https://doi.org/10.1042/BCJ20210301>
43. Janissen R, Murillo DM, Niza B, Sahoo PK, Nobrega MM, Cesar CL, Temperini MLA, Carvalho HF, de Souza AA, Cotta MA. 2015. Spatiotemporal distribution of different extracellular polymeric substances and filamentation mediate *Xyella fastidiosa* adhesion and biofilm formation. *Sci Rep* 5:9856. <https://doi.org/10.1038/srep09856>
44. Siqueira VM, Lima N. 2013. Biofilm formation by filamentous fungi recovered from a water system. *J Mycol* 2013:1–9. <https://doi.org/10.1155/2013/152941>
45. Ophir T, Gutnick DL. 1994. A role for exopolysaccharides in the protection of microorganisms from desiccation. *Appl Environ Microbiol* 60:740–745. <https://doi.org/10.1128/aem.60.2.740-745.1994>
46. Stukalov O, Korenevsky A, Beveridge TJ, Dutcher JR. 2008. Use of atomic force microscopy and transmission electron microscopy for correlative studies of bacterial capsules. *Appl Environ Microbiol* 74:5457–5465. <https://doi.org/10.1128/AEM.02075-07>
47. Whitfield C. 2006. Biosynthesis and assembly of capsular polysaccharides in *Escherichia coli*. *Annu Rev Biochem* 75:39–68. <https://doi.org/10.1146/annurev.biochem.75.103004.142545>
48. Tondo ML, de Pedro-Jové R, Vandecasteyne A, Piskulic L, Orellano EG, Valls M. 2020. KatE from the bacterial plant pathogen *Ralstonia solanacearum* is a monofunctional catalase controlled by HrpG that plays a major role in bacterial survival to hydrogen peroxide. *Front Plant Sci* 11:1156. <https://doi.org/10.3389/fpls.2020.01156>
49. Bär M, Hardenberg J, Meron E, Provenzale A. 2002. Modelling the survival of bacteria in drylands: the advantage of being dormant. *Proc R Soc Lond B* 269:937–942. <https://doi.org/10.1098/rspb.2002.1958>
50. Lebre PH, De Maayer P, Cowan DA. 2017. Xerotolerant bacteria: surviving through a dry spell. *Nat Rev Microbiol* 15:285–296. <https://doi.org/10.1038/nrmicro.2017.16>
51. Grzyb T, Skłodowska A. 2022. Introduction to bacterial anhydrobiosis: a general perspective and the mechanisms of desiccation-associated damage. *Microorganisms* 10:432. <https://doi.org/10.3390/microorganisms10020432>
52. França MB, Panek AD, Eleutherio ECA. 2007. Oxidative stress and its effects during dehydration. *Comp Biochem Physiol A Mol Integr Physiol* 146:621–631. <https://doi.org/10.1016/j.cbpa.2006.02.030>
53. Borisov VB, Siletsky SA, Nastasi MR, Forte E. 2021. ROS defense systems and terminal oxidases in bacteria. *Antioxidants (Basel)* 10:839. <https://doi.org/10.3390/antiox10060839>
54. Gayoso CM, Mateos J, Méndez JA, Fernández-Puente P, Rumbo C, Tomás M, Martínez de Ilarduya O, Bou G. 2014. Molecular mechanisms involved in the response to desiccation stress and persistence in *Acinetobacter baumannii*. *J Proteome Res* 13:460–476. <https://doi.org/10.1021/pr400603f>
55. Farrow JM 3rd, Wells G, Pesci EC. 2018. Desiccation tolerance in *Acinetobacter baumannii* is mediated by the two-component response regulator BfmR. *PLoS One* 13:e0205638. <https://doi.org/10.1371/journal.pone.0205638>
56. Mérida-Floriano A, Rowe WPM, Casadesús J. 2021. Genome-wide identification and expression analysis of SOS response genes in *Salmonella enterica* serovar Typhimurium. *Cells* 10:943. <https://doi.org/10.3390/cells10040943>
57. Cheng J-H, Lv X, Pan Y, Sun D-W. 2020. Foodborne bacterial stress responses to exogenous reactive oxygen species (ROS) induced by cold plasma treatments. *Trends Food Sci Technol* 103:239–247. <https://doi.org/10.1016/j.tifs.2020.07.022>
58. Maier RJ, Benoit SL. 2019. Role of nickel in microbial pathogenesis. *Inorg* 7:80. <https://doi.org/10.3390/inorganics7070080>
59. Reuse H. 2017. Nickel and virulence in bacterial pathogens
60. Tan Z, Chekabab SM, Yu H, Yin X, Diarra MS, Yang C, Gong J. 2019. Growth and virulence of *Salmonella* Typhimurium mutants deficient in iron uptake. *ACS Omega* 4:13218–13230. <https://doi.org/10.1021/acsomega.9b01367>
61. Hori K, Matsumoto S. 2010. Bacterial adhesion: from mechanism to control. *Biochem Eng J* 48:424–434. <https://doi.org/10.1016/j.bej.2009.11.014>
62. Klemm P, Vejborg RM, Hancock V. 2010. Prevention of bacterial adhesion. *Appl Microbiol Biotechnol* 88:451–459. <https://doi.org/10.1007/s00253-010-2805-y>
63. Klemm P, Hancock V, Schembri MA. 2007. Mellowing out: adaptation to commensalism by *Escherichia coli* asymptomatic bacteriuria strain 83972. *Infect Immun* 75:3688–3695. <https://doi.org/10.1128/IAI.01730-06>
64. Roos V, Nielsen EM, Klemm P. 2006. Asymptomatic bacteriuria *Escherichia coli* strains: adhesins, growth and competition. *FEMS Microbiol Lett* 262:22–30. <https://doi.org/10.1111/j.1574-6968.2006.00355.x>
65. Popp PF, Gumerov VM, Andrianova EP, Bewersdorf L, Mascher T, Zhulin IB, Wolf D. 2022. Phyletic distribution and diversification of the phage shock protein stress response system in bacteria and archaea. *mSystems* 7:e0134821. <https://doi.org/10.1128/msystems.01348-21>
66. Wallrodt I, Jelsbak L, Thorndahl L, Thomsen LE, Lemire S, Olsen JE. 2013. The putative thiosulfate sulfurtransferases PspE and GIpE contribute to virulence of *Salmonella* Typhimurium in the mouse model of systemic disease. *PLoS One* 8:e70829. <https://doi.org/10.1371/journal.pone.0070829>
67. Zhou Y, Zhou J, Wang D, Gao Q, Mu X, Gao S, Liu X. 2016. Evaluation of *ompA* and *pgtE* genes in determining pathogenicity in *Salmonella enterica* serovar Enteritidis. *Vet J* 218:19–26. <https://doi.org/10.1016/j.tvjl.2016.10.009>
68. Roy Chowdhury A, Sah S, Varshney U, Chakravorty D. 2022. *Salmonella* Typhimurium outer membrane protein A (OmpA) renders protection from nitrosative stress of macrophages by maintaining the stability of bacterial outer membrane. *PLoS Pathog* 18:e1010708. <https://doi.org/10.1371/journal.ppat.1010708>
69. Kim Y, Wood TK. 2010. Toxins Hha and CspD and small RNA regulator Hfq are involved in persister cell formation through MqsR in *Escherichia coli*. *Biochem Biophys Res Commun* 391:209–213. <https://doi.org/10.1016/j.bbrc.2009.11.033>

70. Pont CL, Bernay B, Gérard M, Dhalluin A, Gravey F, Giard J-C. 2024. Proteomic characterization of persisters in *Enterococcus faecium*. BMC Microbiol 24:9. <https://doi.org/10.1186/s12866-023-03162-8>
71. Deng X, Li Z, Zhang W. 2012. Transcriptome sequencing of *Salmonella enterica* serovar Enteritidis under desiccation and starvation stress in peanut oil. Food Microbiol 30:311–315. <https://doi.org/10.1016/j.fm.2011.11.001>
72. Gruzdev N, McClelland M, Porwollik S, Ofaim S, Pinto R, Saldinger-Sela S. 2012. Global transcriptional analysis of dehydrated *Salmonella enterica* serovar Typhimurium. Appl Environ Microbiol 78:7866–7875. <https://doi.org/10.1128/AEM.01822-12>
73. Liu S, Xue R, Qin W, Yang X, Ye Q, Wu Q. 2023. Performance and transcriptome analysis of *Salmonella enterica* serovar Enteritidis PT 30 under persistent desiccation stress: cultured by lawn and broth methods. Food Microbiol 115:104323. <https://doi.org/10.1016/j.fm.2023.104323>
74. Abdelhamid AG, Yousef AE. 2020. Collateral adaptive responses induced by desiccation stress in *Salmonella enterica*. LWT 133:110089. <https://doi.org/10.1016/j.lwt.2020.110089>
75. Roberts IS. 1996. The biochemistry and genetics of capsular polysaccharide production in bacteria. Annu Rev Microbiol 50:285–315. <https://doi.org/10.1146/annurev.micro.50.1.285>
76. Ai C, Meng H, Lin J, Zhang T, Guo X. 2020. Combined membrane filtration and alcohol-precipitation of alkaline soluble polysaccharides from sugar beet pulp: comparison of compositional, macromolecular, and emulsifying properties. Food Hydrocoll 109:106049. <https://doi.org/10.1016/j.foodhyd.2020.106049>
77. Farhadi F, Khameneh B, Iranshahi M, Iranshahi M. 2019. Antibacterial activity of flavonoids and their structure-activity relationship: an update review. Phytother Res 33:13–40. <https://doi.org/10.1002/ptr.6208>
78. Górniak I, Bartoszewski R, Króliczewski J. 2019. Comprehensive review of antimicrobial activities of plant flavonoids. Phytochem Rev 18:241–272. <https://doi.org/10.1007/s11101-018-9591-z>